Journal of Manufacturing Processes 60 (2020) 418–425

Contents lists available at ScienceDirect

Journal of Manufacturing Processes

journal homepage: www.elsevier.com/locate/manpro

# Ink bridge control in the electrohydrodynamic printing with a coaxial nozzle

Zhen Li [a,b], Karam Nashwan Al-Milaji [b], Hong Zhao [b,*], Da-Ren Chen [a,*]

[a] Particle Laboratory, Department of Mechanical and Nuclear Engineering, Virginia Commonwealth University, Richmond, VA 23284, USA
[b] Micro/nano Transport and Printed Devices Laboratory, Department of Mechanical and Nuclear Engineering, Virginia Commonwealth University, BioTech One, 800 East Leigh Street, Richmond, VA 23219, USA

ARTICLE INFO

*Keywords:*
EHD printing
Coaxial nozzle
Nozzle clogging
Ink bridge control

ABSTRACT

A coaxial nozzle, consisting of two coaxially aligned capillaries to minimize the nozzle clogging (often encountered in a single capillary EHD printing) by enabling continuous ink circulation between the inner and outer ink channels, had been recently proposed for the electrohydrodynamic (EHD) printing. The EHD printing by the coaxial nozzle, however, remains in the early development stage, particularly with respect to the control of ink flow and meniscus during the jetting process. The ink bridge, which connects both openings of the inner and outer capillaries, plays an important role in keeping the ink circulating and influencing the jetting meniscus pinned at the inner capillary tip. In this study, a closed-loop feedback control was developed to automatically regulate the volume of the ink bridge during the printing. It was found that the ink bridge volume affects the volume and shape of the jetting meniscus, which is directly correlated to the printed dot size. Comparing the coaxial printing nozzle to the single capillary nozzle, the addition of the larger outer nozzle does not decrease the printing resolution. The difference in the printed dot diameter between the two printing configurations is less than 5 %. For a given print setting and a specific ink, an optimal ink bridge volume was identified to produce the smallest dot size. With the ink-bridge shape control, the print resolution can be improved by 24.5 %. The correlation between the ink bridge volume, jetting meniscus volume, and the printed dot size also depends on the ink conductivity and the extrusion length of the inner capillary. The coaxial nozzle EHD printing, featuring the continuous ink circulation and effective ink bridge control, provides a reliable manufacturing process in the pattern generation and microfabrication.

## Introduction

Electrohydrodynamic (EHD) jet printing has been employed in the fabrication of microelectronics [1–4], pharmaceutics [5–7], biological tissue structures [8–11], and various functional devices [12–18]. EHD printing has been proven to be a key advancement in the development of high-resolution printing technologies and has good compatibility with a variety of inks and substrates, in addition to all of the attributes of the conventional inkjet printing [19–24]. High-resolution EHD patterning has been achieved by downscaling the size of the printing nozzles (i.e., capillaries) to the micrometer and sub-micrometer ranges. Although the reduction in the nozzle dimensions allows for fine-resolution printing, it also inevitably gives rise to the challenge of severe nozzle clogging.

Nozzle clogging has posed a serious issue in current EHD printing, which uses capillaries with extremely small diameters. The primary reasons for the nozzle clogging include solvent evaporation and ink drying in or near the nozzle tip. Aggregation and precipitation of solid particles (suspended in printing inks) due to solvent evaporation are typically encountered when the inks are kept stagnant at the nozzle tip for a prolonged time period. Therefore, solvent selection must be carefully considered in the ink formulation, even for the conventional inkjet printing, which typically employs printing nozzles with opening diameters of tens of micrometers. For reliable printing, solvents with a low evaporation rate and high solubility are preferred in order to prevent the nozzles from clogging [25–30]. Humectants/surfactants (as additives) are often required to decrease the solvent evaporation rate and to prevent ink particles from aggregation and/or agglomeration [31–34]. In addition, extremely diluted inks are necessary for the EHD printing to minimize the chance of nozzle clogging. The challenges of the intricate ink designs and the frequent nozzle clogging have severely hindered the

* Corresponding author.
*E-mail addresses:* hzhao2@vcu.edu (H. Zhao), dchen3@vcu.edu (D.-R. Chen).

https://doi.org/10.1016/j.jmapro.2020.10.057
Received 16 June 2020; Received in revised form 17 October 2020; Accepted 21 October 2020
Available online 3 November 2020

development of EHD printing into a reliable manufacturing technology.

We have demonstrated an EHD jet printing design featuring continuous ink circulation, enabled by a coaxial nozzle, to mitigate the nozzle clogging which is often encountered in a single capillary EHD printing [35]. The coaxial nozzle, consisting of two concentric capillaries, enables a printing ink to be injected into the inner capillary and withdrawn from the outer capillary at the same time. Keeping the ink circulating at all times largely mitigates the issue of clogging near the EHD printing nozzle tip. The coaxial nozzle EHD printing has demonstrated its capability of printing dot arrays on flexible substrates. However, the printed dots were larger than those produced by a single capillary EHD printing due to poor control of the ink body at the coaxial nozzle tip. In the coaxial nozzle for EHD printing, the inner capillary tip is extruded out from the outer capillary opening. Upon the ink injection into the inner capillary, a flowing ink film is established to bridge both openings of inner and outer capillaries. Depending on the flow rates of the ink feed and withdrawal, the above ink bridge varies significantly in shape and volume, which in turn influences the jetting performance. Although coaxial nozzles have been widely employed in the electrospin and electrospray enabling the micro/nano encapsulation of fibers and particles, respectively [36–48], two fluid streams are injected into two coaxial-aligned flow channels of the nozzles at the same time and form a compound jet at the nozzle exit. Note that, in those applications, the inner capillary of a coaxial nozzle is preferred to be completely immersed in the liquid meniscus pinned at the nozzle exit. To the best of our knowledge, no study has ever been reported on the overall printing performance of a coaxial nozzle when operated under two contra-flowing fluid condition.

In this study, we first compare the jetting formation and meniscus dynamics in the coaxial nozzle EHD printing with that of single capillary printing. A new parameter, i.e., the ink bridge volume, is then introduced and its effect on the jetting meniscus volume and printing performance is investigated. To allow for a reliable printing process against any internal/external disturbances (e.g., flow fluctuation, ink consumption, solvent evaporation, etc.), a closed-loop control of the ink bridge volume and optimization of the printing performance are developed and performed in this study. The sizes of printed dots under various ink bridge volume settings are also further analyzed.

## Experimental method

Fig. 1a shows our experimental setup for the EHD printing with a coaxial nozzle. The coaxial nozzle was constructed by coaxially inserting a fused-silica capillary (the inner channel, TaperTip, New objective) into a stainless-steel tubing (the outer channel) with a thick wall. Three lobe-shaped passages were machined in the wall of the outer capillary for passing liquids and centering the inner capillary (shown in Fig. 1b). The schematic diagram of the coaxial nozzle assembly is shown in Fig. S1. The inner diameter (I.D.) of the outer capillary was made within a tight tolerance to the outer diameter (O.D.) of the inner capillary in order to have enough concentricity between the two capillaries. The inner capillary has an I.D. of 100 μm, a tip O.D. of 154 μm, and a taper of ~ 14° transitioning from the tip to the straight section of the capillary with an O.D. of 360μm. In this study, the nozzle assembly with two extrusion lengths of 900 and 1250 μm, defined as the distance between the exit of inner capillary and the exit of the outer tube, were tested. The reason for the selected extrusion lengths is because, by our experimental observation, a stable ink circulation for the studied nozzle could be established when the extrusion length is set in the range from ~450μm to 1400 μm for the test inks.

The EHD printing system under this study has four subsystems: fluid control, vision acquisition, motion control, and power supply. Four subsystems were integrated to enable the continuous ink-circulation and automatically control the ink bridge volume to offer robust EHD printing.

### *Fluid control*

The printing ink used in this work is given in the supporting information (SI). The pressure feed and vacuum withdrawal of printing inks were implemented in our setup to facilitate continuous and stable ink circulation for the operation of the coaxial nozzle. Compared to the syringe pump feeding used in previous studies, the pressure-based fluid driving offers a clear advantage (in the stability of ink delivery) on regulating and maintaining the ink meniscus shape, particularly for the coaxial nozzle EHD printing. Although the ink circulation could reach a new equilibrium status via the use of syringe pumps set at the fixed infusion and withdrawal rates, the ink consumption as the jetting proceeds would likely disturb the balance of ink circulation over a long printing period. Printing variable data (which requires various ink consumption rates) poses an additional challenge in keeping the ink bridge shape and meniscus stable. The infusion and/or withdrawal rates of the syringe pumps are required to be adjusted in real-time to meet the requirement of varying ink consumption rates and ink circulation. Moreover, the slow response of the jetting meniscus after setting new flow rates on syringe pumps makes it difficult to meet the above printing demands. The flow pulsation caused by the stepping motors in syringe pumps also makes it challenging to achieve and maintain a stable ink

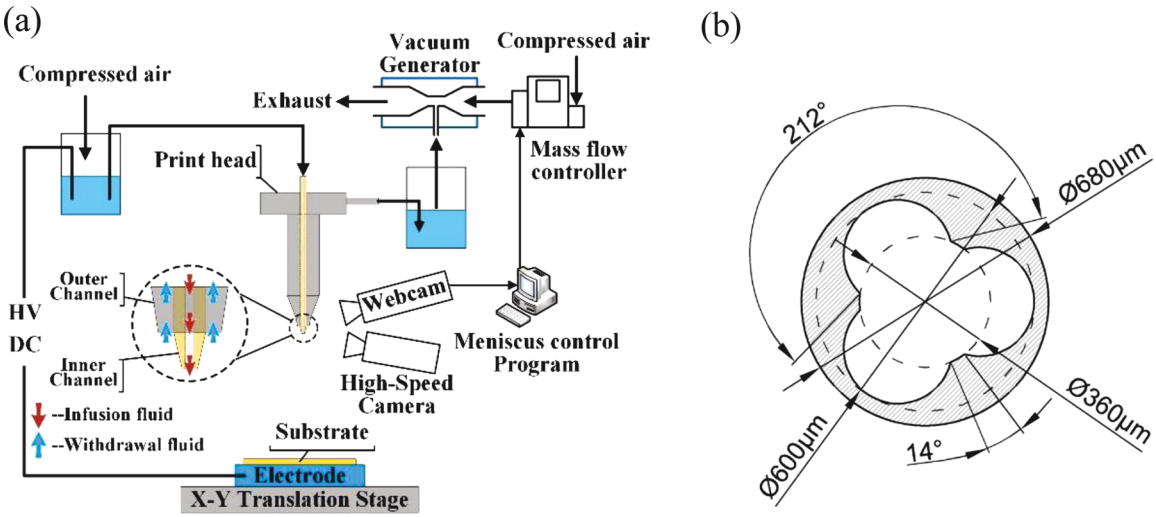


**Fig. 1.** (a) Schematic diagram of the experimental setup for the coaxial EHD printing. (b) The cross-sectional view of the outer capillary.

bridge, particularly at low flow rate settings. To address the previously discussed technical challenges in maintaining a stable meniscus shape during the coaxial nozzle EHD printing, pressure-based ink feed and withdrawal were developed for the fluid control in our setup.

The fluid control subsystem consists of two cylindrical chambers, compressed air lines, and pressure regulators. Two cylindrical chambers, one set at positive pressure for ink feeding and the other at negative pressure for ink withdrawal, were constructed. The positive and negative pressure chambers are connected to the inner and outer capillaries in the coaxial nozzle, respectively. A precision pressure regulator controls the compressed air to the positive pressure chamber at the air pressure of ~ 1.0 psi. Under the pressure setting given above, the ink feeding rate was calculated at 7.93 μL/min (using the Poiseuille equation for fully developed flow in round pipes). An ejector vacuum (Air-Vac Engineering, AVR038 H) was applied to create negative pressure in the ink withdrawal chamber, providing a vacuum to the outer capillary of the coaxial nozzle. Compressed air to operate the ejector vacuum is controlled by a mass flow controller (Alicat Scientific, MC-20SLPM-D). The vacuum level in the negative pressure chamber to control the ink withdrawal rate was adjusted through varying the air flow rate supplied to the ejector vacuum. Combined with the closed-loop control of the ink bridge (details to be described in the next section), this fluid control subsystem allows for a reliable EHD printing process with continuous ink circulation to accommodate the variation of ink consumption rates due to such changes as variable data printing and solvent evaporation.

*Closed-loop control of ink bridge*

When the continuous ink circulation is enabled in the coaxial nozzle, printing ink flows from the outlet opening of the inner capillary to the inlet opening of the outer capillary, resulting in the ink body. This ink body is composed of the jetting meniscus (pinned at the tip of the inner capillary) and the ink bridge (connecting the pinned meniscus to the outer channel opening; Fig. 2a, b) at the nozzle tip. A closed-loop control was developed in this work to automatically control the shape of the ink bridge. The control of ink bridge can be in general accomplished by regulating both ink feed and withdrawal flow rates. For the simplicity and demonstration, we controlled the ink withdrawal flow rate while keeping the ink injection flow rate constant. The flow chart of the above control is shown in Fig. 2c. Prior to each run, the system was operated for a short period of time to find the ink bridge shape offering the reliable printing quality. The image of the above-identified ink bridge was then taken by a web camera (Fig. 2a) and saved as the pre-selected reference. During the run, the image of the ink bridge was continuously taken and compared to the pre-selected reference. If the imaged shape of the ink bridge (defined by the ratio of dark to bright areas) is different from the reference, an adjustment in the ink withdrawal flow rate would be made to regulate the vacuum pressure level in the associated chamber. More ink flow would be drawn into the ink withdrawal chamber if the chamber pressure level was reduced. In the opposite case, less ink flow would be drawn into the chamber. The chamber vacuum pressure was varied through the control of the mass flow rate of an air-ejector pump which was connected to the ink withdrawal chamber. The

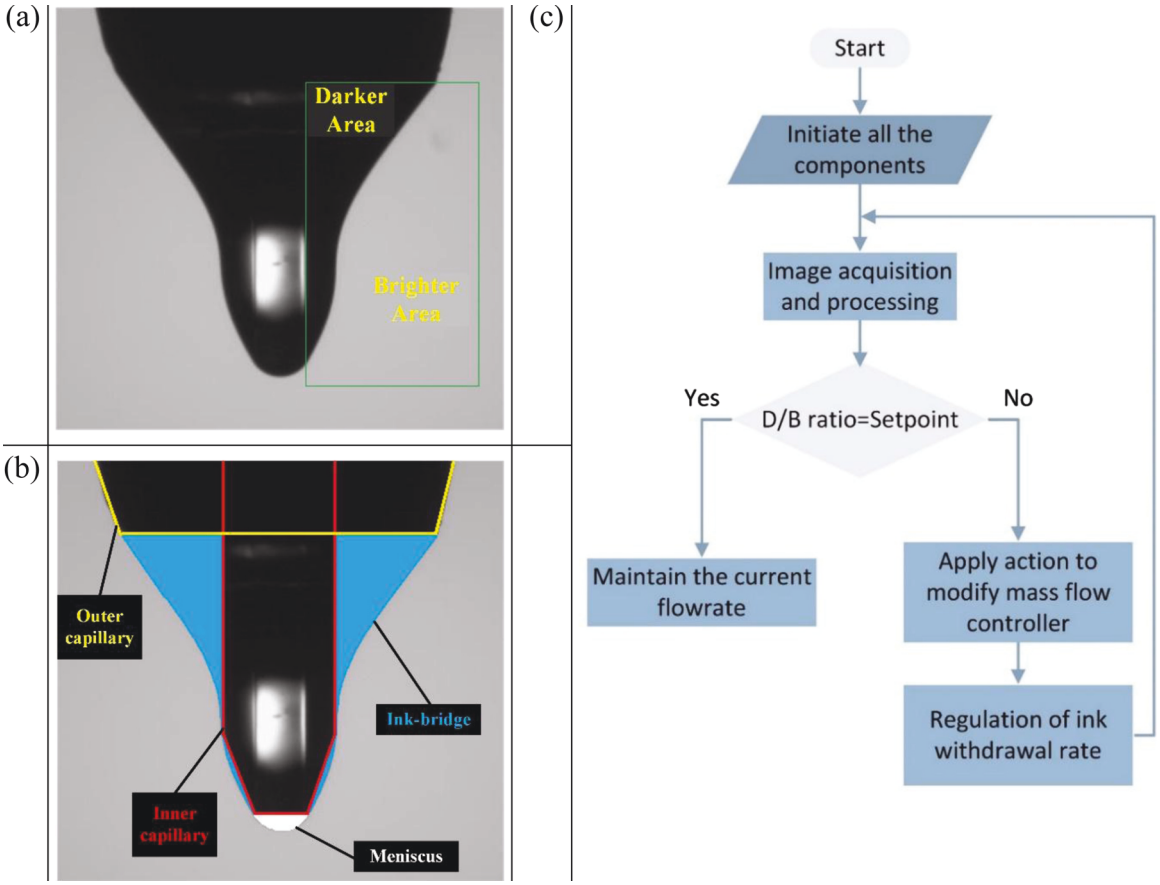


**Fig. 2.** (a) The image of the ink bridge under the monitoring process. In the region of interest (ROI), which is labeled with a green box, the ink bridge area is referred to the dark area. The gray background in the rest of the ROI is referred to the bright area. (b) A schematic of the ink bridge connecting the inner and outer capillary openings, which allows for continuous ink circulation, and the jetting meniscus, which is subjected to the electric field for droplet generation. (c) A process diagram of the closed-loop feedback control of the ink bridge shape. The pixel ratio of the dark area to the bright area in the ROI (D/B) is taken as the processing variable and compared to the setpoint (the pre-defined reference) (For interpretation of the references to colour in this figure legend, the reader is referred to the web version of this article).

adjustment to the mass flow rate for operating the air pump was controlled by a mass flow controller which is commended by the control code developed in LabVIEW. The real-time imaging and automatic regulation of ink bridge volume also allows us to keep the ink bridge intact during printing.

LabVIEW (National Instruments) was used to program the closed-loop control to be usable with a computer interface (as shown in Fig. S2). This closed-loop control program consists of fluid flow and vision modules working in parallel. The fluid flow module controls the flow rate of compressed air to the ejector vacuum pump, varying the vacuum level in the ink withdrawal chamber. The vision module acquires the image of the ink bridge via a web camera. Once an image is taken with the web camera, the NI Vision Acquisition Software (VAS) then analyzes the image by calculating the number of pixels in the ink bridge area (the dark area) and the non-ink bridge area (the bright area). Adjustments to the flow rate setting for the mass flow controller are calculated based on the difference between the desired dark-to-bright pixel ratio (i.e., the setpoint) and the measured ratio (i.e., the process variable). The updated flow rate setting is then sent to the flow module to change the vacuum in the negative pressure chamber.

The closed-loop control automatically adjusts the ink withdrawal when the ink bridge shape (or volume) falls out of the user-defined pixel ratio range. As an example (shown in Fig. S3), an artificial disturbance was introduced by wiping out the ink at the nozzle tip using a foam swab. With the closed-loop control in place, it took ~4–5 seconds to restore the pre-selected ink bridge shape. Note that the artificial disturbance introduced above was only for the purpose of illustrating the developed closed-loop control and would otherwise be considered a large interruption, which would not be encountered in the typical operation of the coaxial nozzle. Gradual changes of the ink bridge shape caused either by the ink consumption or solvent evaporation are more typical in the normal operation of coaxial nozzle EHD printing.

*Vision acquisition*

A 1.3-megapixel (using a frame rate of 16 fps) web camera (Edmunds Optical EO-3112C) and a 12X zoom lens (Navitar) were used to capture the ink bridge image during the printing. In addition, a high-speed camera (Phantom, Miro 3a10, at the frame rate of 35k fps) with a microscopic lens (Infinity Model K2 DistaMax) was employed to monitor the dynamics of the ink meniscus at the nozzle tip. One LED light source was utilized to illuminate the viewing areas of both cameras.

*Power supply*

A high pulse voltage, created by superimposing a pulse voltage onto an offset DC voltage, was used to produce on-demand ink droplets. The high voltage was applied to the moving stage while the coaxial nozzle was electrically grounded. A function generator (Fluke, Model 282) was used to provide the input signal for the high-voltage amplifier (Matsusada Precision, AMT-20B10-LCN1) to generate various printing sequences, while the amplitude and frequency of the printing voltage sequences were monitored by an oscilloscope (Agilent, 54622A).

*Motion control*

Polyethylene terephthalate (PET) films (Mitsubishi Paper Mills, NB-TP-3GU100) with a thickness of 135 μm were used in our EHD printing. The PET films were sputtered with gold to achieve the measured sheet resistance of 482.29 Ohms per square. Two translational stages (Thorlabs, MTS25-Z8) moved the target substrate in the X and Y directions for dot array patterning.

## Result and discussion

*Comparison of performance between the coaxial and single capillary nozzles*

In this part of the study, we compare the droplet formation and printed dot sizes in EHD printing between the coaxial nozzle and single capillary nozzles. The drop-on-demand jet process was used for testing conventional single capillary EHD printing. A pulse voltage (3.2 kV with the 200 μs duration) was applied to pull the ink out by deforming the originally round meniscus into a conical shape (Fig. 3a). A thin filament is emitted from the cone apex once the pulse voltage was applied, and quickly pinches off at the end of the applied pulse voltage. A droplet is thus formed from the broken filament (due to surface tension) and the pinched-off droplet travels downwards and is deposited on the substrate because of its inertial momentum and the applied electrical field. To test single capillary nozzle performances, the outer and inner capillaries of the coaxial nozzle were used individually. In testing single capillary printing with the inner capillary, the extruded inner capillary with no ink circulation (i.e., the outer capillary being blocked) was employed. For testing with the only outer capillary, the inner capillary was completely retracted inside the outer one (in Fig. 3b). The volume and shape of the jetting meniscus were very different between the tested printing cases. The large volume of the ink meniscus at the capillary tip is responsible for the generation of large droplets. Note that it is impossible to actuate this printing using the same pulse voltage setting adopted in printing with only the inner capillary (due to the large meniscus volume). A pulse voltage (4.5 kV) and a long pulse duration (3000 μs) were necessary to produce single droplets in this case.

The printing with the coaxial nozzle (with the ink circulation feature on) is shown in Fig. 3c. The geometrical and operational settings for this printing, e.g., the nozzle-to-substrate distance, voltage magnitude and pulse width, net delivered ink volume, etc., were the same as those in the case with the inner-capillary-only printing. The images in Fig. 3c show that the ink body at the nozzle tip could be partitioned into two areas: the jetting meniscus area and the ink bridge area. The jetting meniscus pinned at the tip of the inner capillary is graphically defined in Fig. S4. During the meniscus and droplet formation, the ink bridge was insensitive by the variation of applied voltage (because the electric field was mostly concentrated around the inner capillary tip). Correspondingly, electrical charges were mostly concentrated at the surface of the jetting meniscus when compared to that of the surface of the ink bridge.

The printed dot sizes on the PET substrate were measured under various printing conditions. The fluorescence images of dots from printing using only the inner and outer capillary respectively, and the coaxial nozzle are shown in Fig. 3d–f, respectively. The dots printed by the single outer capillary (Fig. 3g) have an average diameter of 321.3 μm, which are significantly larger than those printed by the other two nozzle configurations. Due to the large meniscus established in the outer capillary printing, the formation of the conical shape at the beginning of each jetting cycle was significantly delayed even when a stronger electric field was applied (compared to that of the two other printing nozzle cases). An extended pulse duration was also required to pull a droplet out of the jetting meniscus and to restore the meniscus shape. These conditions resulted in the observation of large dots, a long jetting period (i.e., low jetting frequency), and wide dot spacing on the image shown in Fig. 3e.

The printed dot sizes obtained from printing using the inner capillary only are comparable to that of the coaxial nozzle. Average dot sizes of $90.1 \pm 1.42$ and $94.6 \pm 1.21$ μm were measured in the printing using the coaxial nozzle and the singular inner capillary, respectively. The close size result is due to the employment of the same capillary as the jetting head, where the printed dot size is mainly determined by the meniscus shape and volume when the same ink and printing settings are used. In the EHD printing using only the inner capillary, the ink meniscus pinned at the capillary tip was subject to electric field application. A droplet was

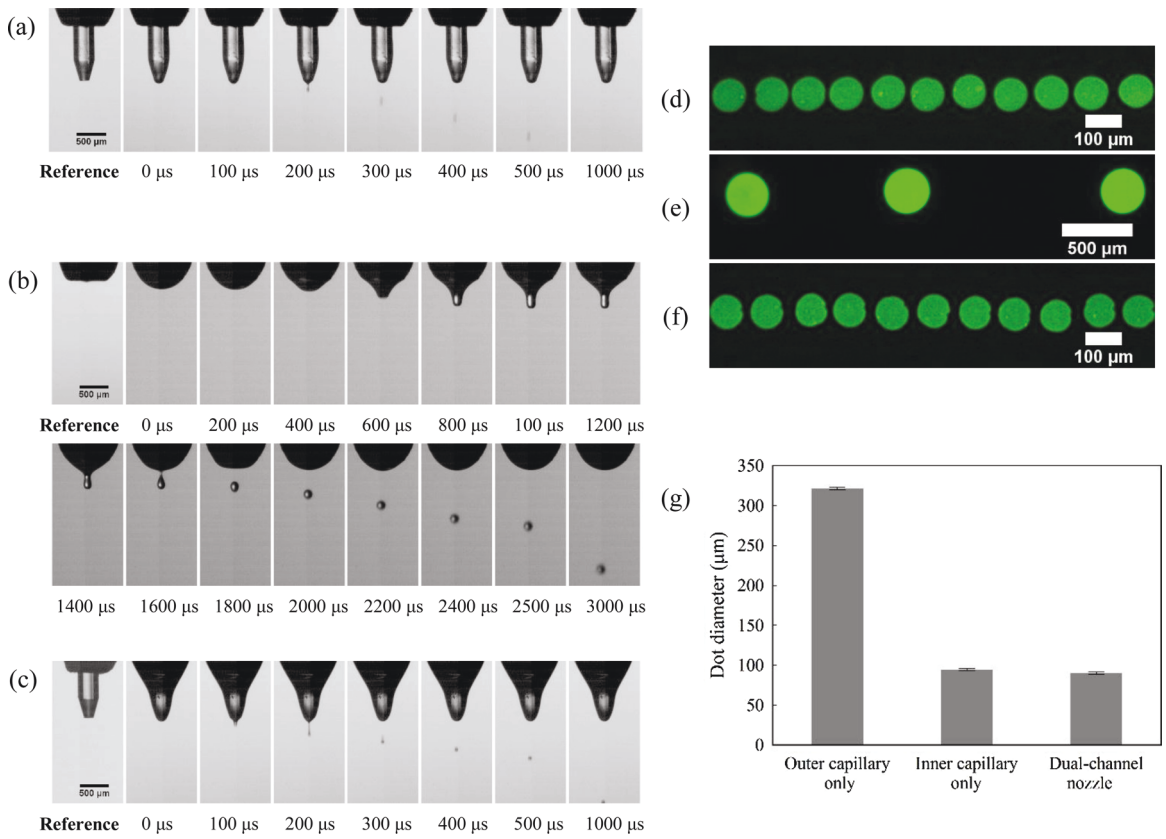


**Fig. 3.** Time-resolved images of the jetting formation with different nozzle configurations: (a) Single inner capillary only ($V_{dc} = 1.0$ kV, $V_{pulse} = 3.2$ kV, Pulse width = 200 μs); (b) single outer capillary only ($V_{dc} = 1.6$ kV, $V_{pulse} = 4.5$ kV, Pulse width = 1600 μs), (c) coaxial nozzle ($V_{dc} = 1.0$ kV, $V_{pulse} = 3.2$ kV, Pulse width = 200 μs). (d)–(f) Fluorescence microscope images of printed dots from the single inner and outer capillaries, and the coaxial nozzle, respectively. (g) Comparison of the printed dot sizes from the three printing nozzle configurations.

ejected at the capillary tip when enough electrical force was applied on the ink meniscus. In contrast, in the coaxial EHD printing, the EHD jetting (involving the formation of conical shape for the droplet ejection) was largely confined to the tip of the inner capillary. The ink bridge was not directly involved in the jetting, although its shape (and volume) does affect the jetting meniscus volume (to be discussed in the next section). The primary function of the outer capillary in the coaxial nozzle is thus for maintaining continuous ink circulation. As shown, the coaxial nozzle can produce droplets in sizes comparable to that by a single capillary nozzle, with the added benefit of mitigating nozzle clogging.

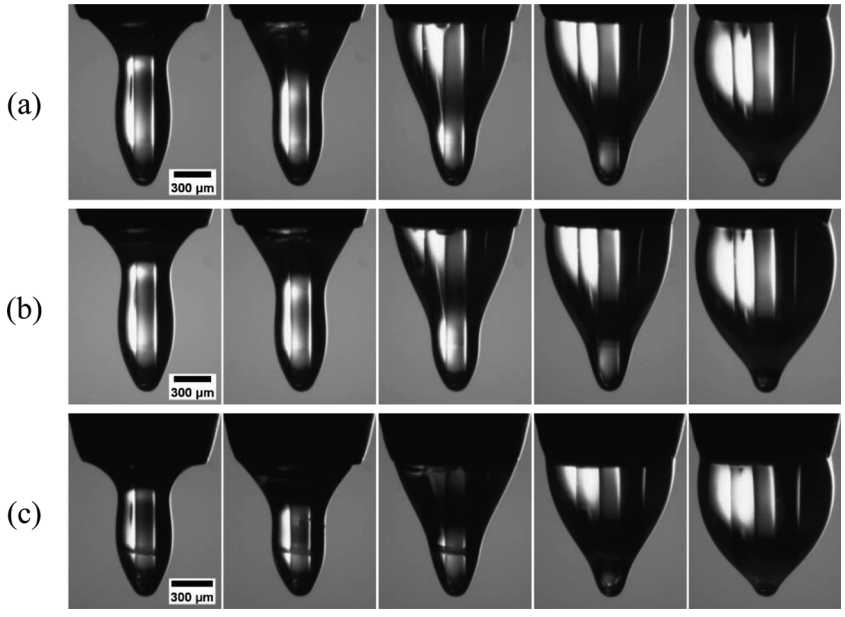


**Fig. 4.** Images of the shape evolution of the ink bridges in coaxial EHD printing with the two electrical conductivities of ink and two extrusion lengths of inner capillary: (a) 565 μS/cm – 1250 μm, (b) 965 μS/cm – 1250 μm, (c) 965 μS/cm – 900 μm.

*Effect of Ink bridge volume on the jetting behavior*

Since the jetting meniscus is pinned at the inner capillary tip, its volume is largely determined by the O.D. of the inner capillary tip in the coaxial nozzle. The flowing ink film bridging the inner and outer capillary openings also affects the shape and volume of the jetting meniscus. The volume of the ink bridge then influences the elongation and volume of the jetting meniscus, thus affecting the size of printed dots. In this part of the study, the ink bridge volume was varied by the closed-loop control to investigate its effect on the jetting behavior. For the configuration of the coaxial nozzle, two extrusion lengths of 900 and 1250 μm (measured from the opening of the inner capillary to the opening of the outer capillary) were selected and printing inks with two different conductivities (i.e., 565 and 965 μS/cm) were employed. The ink bridge volume was gradually varied by the developed feedback control, as shown in Fig. 4. The nozzle-to-substrate distance and the applied voltage (a pulse voltage superimposed onto a DC voltage) remained unchanged for all the printing conditions (i.e., $V_{dc} = 1.22$ kV, $V_{pulse} = 3.62$ kV, and pulse duration = 105 μs). The ink bridge volume was calculated based on the images taken by the web camera. The detailed calculation method can be found in the Supporting Information (Fig. S5). The jetting meniscus volume at the end of the pulse voltage (and prior to the droplet ejection) was calculated by analyzing the image taken by the high-speed camera (taking the opening of the inner capillary as the reference line).

Fig. 5 shows the jetting meniscus volume as a function of the ink bridge volume under the coaxial nozzle printing with two extrusion length settings. It was found that the jetting meniscus volume initially decreases as the ink bridge volume increases, and then increases as the ink bridge volume further increases. When the coaxial nozzle is operated, the ink flows from the inner capillary opening to the outer capillary opening and covers the outer wall of the extruded inner capillary, i.e., the tapered tip and straight sections (Fig. 2b). The climbing ink on the outer wall of the extruded capillary is primarily driven by the vacuum from the ink withdrawal chamber. Given a specific ink bridge volume setting, various forces, i.e., suction vacuum, ink viscous force, ink surface tension, electrical forces act on the ink bridge and must be balanced in order to reach a stable shape, hence the need for modulating the base of the jetting meniscus. An optimal ink bridge volume (which gave the smallest jetting meniscus) was observed in Fig. 5. Below this optimal ink bridge volume, (e.g., the 1st column in Fig. 4), the average thickness of the ink bridge was thin and the base of the jetting meniscus expanded in order to minimize the intensity of the electrical field at the outer corner of the extruded capillary, resulting in ink accumulation at the inner capillary tip. Further reduction of the ink bridge volume caused bifurcation of the flowing film (i.e., failure for ink circulation); in other words, a minimal ink bridge volume is required to keep the continuous ink circulation. When the ink bridge volume was allowed to be higher than the optimal volume, the thickness of the ink bridge film increased (due to the increased volume), resulting in the increased base of the jetting meniscus and its volume. The thick ink film adjacent to the base of the jetting meniscus also reduced the electric field intensity that occurred at the outer corner of the inner capillary.

As shown in Fig. 5a, the characteristics of the jetting meniscus volume curve observed above remain the same when the ink conductivity was increased. It was found that the higher ink conductivity, the larger jetting meniscus. As the pulse voltage was applied, the jetting meniscus elongated into a conical shape, driving a portion of the liquid in the ink bridge (adjacent to the jetting meniscus base) toward the inner capillary tip. Because of the increased electrical conductivity, the electrical charge density on the ink surface is also increased, making the ink bridge more likely to be influenced by the applied pulse voltage. As a result, a larger jetting meniscus volume was obtained with the high conductivity ink compared to that of low conductivity ink.

Compared to the case with the extrusion length of 1250 μm, the ink bridging the openings of inner and outer channels significantly changed its shape in the printing with the nozzle with a short inner capillary extension length, i.e., 900 μm (Fig. 5b). For a certain jetting meniscus volume, the short inner capillary extrusion length results in a thick ink bridge film. Under the same ink bridge volumes, the nozzle with the short extrusion length leads to the significant decrease of the jetting meniscus volume (compared to that in the case with the long extrusion length). Consequently, the jetting meniscus is less affected by the ink bridge in the short extrusion configuration. Note that the jetting meniscus volume abruptly decreased at the maximal ink-bridge volume setting (due to the unstable jetting). As shown in the last image in Fig. 4c, the ink bridge was so large that the jetting meniscus could not be effectively pinned at the inner capillary tip, representing the transition to single outer capillary printing (Fig. 3b). The pulse voltage attempted to actuate the entire ink body (ink bridge and jetting meniscus) but could not complete the droplet ejection (Fig. S6). When combining low conductivity ink with short extrusion length (i.e., 565 μS/cm and 900 μm extrusion), the applied pulse voltage was inadequate to eject a droplet due to the weak electrostatic actuation and the possible depinning of the jetting meniscus. It is further noted that, in all the test cases, the optimal ink bridge volume was $\sim 3.0 \times 10^{-13}$ cm$^3$, probably due to the tapered tip of the inner capillary.

The footprint of produced droplets on the substrate (i.e., flat and circular dots) was used to evaluate the print resolution of the coaxial nozzle EHD printing. The printed dots were made of fluorescein salt after the solvent evaporation, making them easy to be characterized by a fluorescent tracer. Fig. 6 shows how the printed dot size monotonically

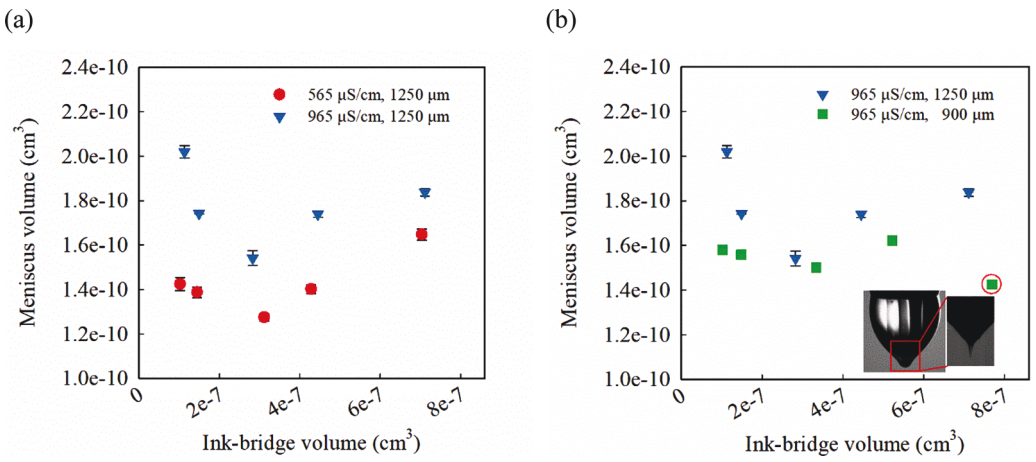


**Fig. 5.** Meniscus jetting meniscus volume with respect to the ink bridge volume for EHD printing using coaxial nozzles: (a) with two inks of different conductivities; (b) having two different extrusion lengths for the inner capillary.

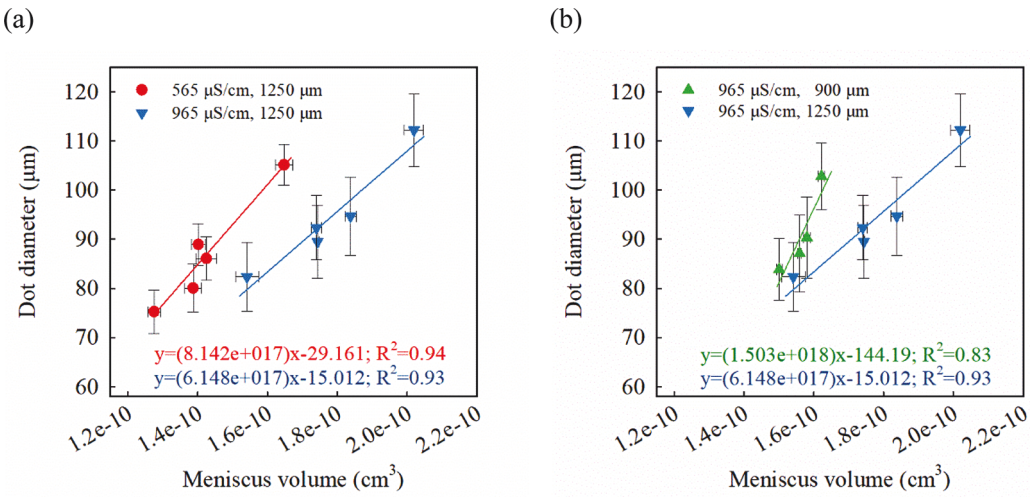


**Fig. 6.** The printed dot sizes with respect to their corresponding meniscus volume with (a) different ink conductivities, and (b) different extrusion lengths of the inner capillary.

increases with the increase of the jetting meniscus volume under the three different printing settings. The measured dot sizes on the substrate were between 75.22 ± 4.42 and 112.19 ± 7.39 μm. The smallest dot size corresponds to the smallest ink bridge volume (i.e., the optimal ink bridge volume) for each printing condition. Three clearly distinguishable fitting curves show that the monotonical correlation is applicable to each case but the slope of correlation lines is uniquely dependent on the specific ink formulation and the printing conditions (i.e., ink conductivity, inner capillary extrusion length, etc.). These results show that, for a given printing configuration, the most straightforward mean to vary the dot size is through the control of jetting meniscus volume (or the ink bridge volume).

Fig. 6a shows the linear relationship between the jetting meniscus volume and the dot diameter when using inks with different electrical conductivities. Using the same inner capillary extrusion length, the slope of the dot diameter with respect to the jetting meniscus volume in the high conductivity ink case is similar to that of the low ink conductivity case. For the same jetting meniscus volume, large dots were generated in the case of low conductivity ink, because when the pulse voltage was applied, the jetting meniscus elongated into a cone, leading to charge accumulation at the cone tip. When the Coulomb force overcame the ink surface tension, the resultant instability broke the meniscus tip apart and formed a charged droplet (by the ink surface tension). Because of its low surface charge density, the low conductivity ink meniscus required more time to accumulate enough surface charge density prior to the droplet pinch-off (Fig. S7), leading to the ejection of a larger droplet. By the same mechanism, a small droplet can easily be emitted from the jetting meniscus using high conductivity ink. Moreover, it is interesting to observe that, when operated at the optimal ink bridge setting (i.e., the smallest meniscus volumes), the printed dot sizes in both ink cases are similar to each other.

Comparing the nozzles with different inner capillary extrusion lengths (Fig. 6b), the line slope of the dot diameter with respect to the jetting meniscus volume in the case with the 900 μm extrusion length is very different from that in the case with the extrusion length of 1250 μm. As discussed above, the ink bridge in the nozzle with the short extrusion length tends to be thicker than that of the nozzle with the long length, resulting in the small jetting meniscus volume in the latter nozzle. The dot size quickly increased as the jetting meniscus volume increased, probably due to the less effective meniscus pinning at the inner capillary tip. Again, when operated at their optimal ink bridge conditions (i.e., the smallest meniscus volumes), the printed dot sizes in both nozzle configuration cases are very similar to each other. This result once again lends support to the recommendation of operating the coaxial nozzle near the optimal ink bridge volume setting. Not only does using the optimal ink bridge volume setting achieve stable jetting and minimal dot sizes, but it also produces droplets insensitive to the extrusion length and the electrical conductivity of the inks.

Note that the same pulse voltage setting was employed in all the printing cases reported in this work (for the sake of comparison). However, the voltage setting used may not be the optimal one for each case. Using a pulse voltage with a reduced magnitude and duration to that of the one used in this study, a coaxial nozzle with an inner capillary of an even smaller diameter (both OD and ID) can be expected to produce very small dots.

## Conclusion

We have demonstrated that coaxial nozzle EHD printing can generate dot sizes comparable to that of single capillary EHD printing while enabling continuous ink circulation for reducing the risk of nozzle clogging. The real-time feedback control of the ink bridge shape has been developed to regulate the ink circulation against any disturbances during the printing process. The effect of the ink bridge in the coaxial nozzle on the jetting meniscus formation and printing performance was investigated and it was found that the printed dot size directly correlates with the volume of the jetting meniscus: the smaller the jetting meniscus volume, the smaller the printed dot size. No monotonic relationship between the ink bridge and the jetting meniscus volumes was observed. Instead, the jetting meniscus volume first decreases to a minimum and then increases as the ink bridge volume increases. As a result, an optimal ink bridge volume (where the smallest jetting meniscus volume is present) for a given print setting with a specific ink formulation exists, in which the minimal dot size can be obtained. Moreover, when the printing is done at the optimal ink bridge volume, the printed dot size is insensitive to the ink conductivity and the extrusion length of the inner capillary in the coaxial nozzle. The closed-loop feedback control of the ink bridge shape enables users to quickly determine the optimal printing operation settings in addition to maintaining a stable printing process. This study has made a significant contribution in advancing coaxial nozzle EHD printing into a reliable manufacturing technology.

The focus of this study is on the evaluation of the printing performance of coaxial nozzle EHD printing when operated at the on-demand mode. The flat and circular dotted patterns were thus produced to evaluate the footprint of droplets after deposited on the substrates. The application of coaxial nozzle EHD printing to produce novel structures will be our focus of the future research.

## Declaration of Competing Interest

The authors report no declarations of interest.

## Acknowledgements

We are grateful to Huanqing Wang and Wangjin Xia for their invaluable assistance with the control software development. This research is financially supported by the National Science Foundation (Grant No. CMMI-1726627).

## Appendix A. Supplementary data

Supplementary material related to this article can be found, in the online version, at doi:https://doi.org/10.1016/j.jmapro.2020.10.057.

## References

[1] Sekitani T, Noguchi Y, Zschieschang U, Klauk H, Someya T. Organic transistors manufactured using inkjet technology with subfemtoliter accuracy. Proc Natl Acad Sci USA 2008;105:4976–80.
[2] Jang Y, Kim J, Byun D. Invisible metal-grid transparent electrode prepared by electrohydrodynamic (EHD) jet printing. J Phys D Appl Phys 2013;46:155103.
[3] Kim K-W, Oh H, Bae JH, Kim K-W, Moon HC, Kim K-W. Electrostatic-force-Assisted dispensing printing of electrochromic gels for low-voltage displays. ACS Appl Mater Interfaces 2017;9:18994–9000.
[4] Kim K, Bae J, Noh SH, Jang J, Kim SH, Park CE. Direct writing and aligning of small-molecule organic semiconductor crystals via “Dragging mode” electrohydrodynamic jet printing for flexible organic field-effect transistor arrays. J Phys Chem Lett 2017;8:5492–500.
[5] Enayati M, Chang M-W, Bragman F, Edirisinghe M, Stride E. Electrohydrodynamic preparation of particles, capsules and bubbles for biomedical engineering applications. Colloids Surf A Physicochem Eng Asp 2011;382:154–64.
[6] Zamani M, Prabhakaran MP, Ramakrishna S. Advances in drug delivery via electrospun and electrosprayed nanomaterials. Int J Nanomedicine 2013;8:2997–3017.
[7] Wei C, Dong J. Direct fabrication of high-resolution three-dimensional polymeric scaffolds using electrohydrodynamic hot jet plotting. J Micromech Microeng 2013;23:025017.
[8] Luca G, Devid M, Antonella M, Claudio M. An electrohydrodynamic bioprinter for alginate hydrogels containing living cells. Tissue Eng Part C Methods 2015;21:123–32.
[9] Derby B. Printing and prototyping of tissues and scaffolds. Science 2012;338:921–6.
[10] Kim K, Lee BU, Hwang GB, Lee JH, Kim S. Drop-on-Demand patterning of bacterial cells using pulsed jet electrospraying. Anal Chem 2010;82:2109–12.
[11] Jayasinghe SN, Qureshi AN, Eagles PAM. Electrohydrodynamic jet processing: an advanced electric-field-Driven jetting phenomenon for processing living cells. Small 2006;2:216–9.
[12] Hyungdong L, Baekhoon S, Jihoon K, Yonghee J, Doyoung B. Direct alignment and patterning of silver nanowires by electrohydrodynamic. Jet Printing Small 2014;10:3918–22.
[13] An BW, Kim K, Kim M, Kim SY, Hur SH, Park JU. Direct printing of reduced graphene oxide on planar or highly curved surfaces with high resolutions using electrohydrodynamics. Small 2015;11:2263–8.
[14] Wang J-C, Zheng H, Chang M-W, Ahmad Z, Li J-S. Preparation of active 3D film patches via aligned fiber electrohydrodynamic (EHD) printing. Sci Rep 2017;7:43924.
[15] An BW, Kim K, Lee H, Kim S-Y, Shim Y, Lee D-Y, Song JY, Park J-U. High-resolution printing of 3D structures using an electrohydrodynamic inkjet with multiple functional inks. Adv. Mater 2015;27:4322–8.
[16] Kim BH, Onses MS, Lim JB, Nam S, Oh N, Kim H, Yu KJ, Lee JW, Kim J-H, Kang S-K, Lee CH, Lee J, Shin JH, Kim NH, Leal C, Shim M, Rogers JA. High-resolution patterns of quantum dots formed by electrohydrodynamic jet printing for light-emitting diodes. Nano Lett 2015;15:969–73.
[17] Wang DZ, Jayasinghe SN, Edirisinghe MJ. High resolution print-patterning of a nano-suspension. J Nanopart Res 2005;7:301–6.
[18] Shigeta K, He Y, Sutanto E, Kang S, Le A-P, Nuzzo RG, Alleyne AG, Ferreira PM, Lu Y, Rogers JA. Functional protein microarrays by Electrohydrodynamic jet printing. Anal Chem 2012;84:10012–8.
[19] Zhang B, He J, Li X, Xu F, Li D. Micro/nanoscale electrohydrodynamic printing: from 2D to 3D. Nanoscale 2016;8:15376–88.
[20] Onses MS, Sutanto E, Ferreira PM, Alleyne AG, Rogers JA. Mechanisms, capabilities, and applications of high-resolution electrohydrodynamic jet printing. Small 2015;11:4237–66.
[21] Park J-U, Hardy M, Kang SJ, Barton K, Adair K, D k Mukhopadhyay, Lee CY, Strano MS, Alleyne AG, Georgiadis JG, Ferreira PM, Rogers JA. High-resolution electrohydrodynamic jet printing. Nat Mater 2007;6:782.
[22] Singh M, Haverinen HM, Dhagat P, Jabbour GE. Inkjet printing-process and its applications. Adv. Mater 2010;22:673–85.
[23] Yogi O, Kawakami T, Yamauchi M, Ye JY, Ishikawa M. On-demand droplet spotter for preparing pico- to femtoliter droplets on surfaces. Anal Chem 2001;73:1896–902.
[24] Onses MS, Song C, Williamson L, Sutanto E, Ferreira PM, Alleyne AG, Nealey PF, Ahn H, Rogers JA. Hierarchical patterns of three-dimensional block-copolymer films formed by electrohydrodynamic jet printing and self-assembly. Nat Nanotechnol 2013;8:667–75.
[25] Calvert P. Inkjet printing for materials and devices. Chem Mater 2001;13:3299–305.
[26] Molesa S, Redinger DR, Huang DC, Subramanian V. High-quality inkjet-printed multilevel interconnects and inductive components on plastic for ultra-low-cost RFID applications. Mater Res Soc Symp Proc 2003;769(H8):3.
[27] Hoth CN, Choulis SA, Schilinsky P, Brabec CJ. High photovoltaic performance of inkjet printed polymer:fullerene blends. Adv Mater 2007;19:3973–8.
[28] Nallan HC, Sadie JA, Kitsomboonloha R, Volkman SK, Subramanian V. systematic design of jettable nanoparticle-based inkjet inks: rheology, acoustics, and jettability. Langmuir 2014;30:13470–7.
[29] Chen S-P, Chiu H-L, Wang P-H, Liao Y-C. Inkjet printed conductive tracks for printed electronics. ESC J Solid State Sci Technol 2015;4. P3026-P33.
[30] Kwon J, Hong S, Suh YD, Yeo J, So H-M, Chang WS, et al. Direct Micro metal patterning on plastic substrates by electrohydrodynamic jet printing for flexible electronic applications. ESC J Solid State Sci Technol 2015;4. P3052-P6.
[31] Park J-U, Lee JH, Paik U, Lu Y, Rogers JA. Nanoscale patterns of oligonucleotides formed by electrohydrodynamic jet printing with applications in biosensing and nanomaterials assembly. Nano Lett 2008;8:4210–6.
[32] Li J, Rossignol F, Macdonald J. Inkjet printing for biosensor fabrication: combining chemistry and technology for advanced manufacturing. Lab Chip 2015;15:2538–58.
[33] Steirer KX, Berry JJ, Reese MO, van Hest MFAM, Miedaner A, Liberatore MW, Collins RT, Ginley DS. Ultrasonically sprayed and inkjet printed thin film electrodes for organic solar cells. Thin Solid Films 2009;517:2781–6.
[34] Formation of conductive silver films via inkjet reaction systemKao Z-K, Hung Y-H, Liao Y-C, editors. J Mater Chem 2011;21:18799–803.
[35] Li Z, Al-Milaji KN, Zhao H, Chen D-R. Electrohydrodynamic (EHD) jet printing with a circulating dual-channel nozzle. J Micromech Microeng 2019;29:035013.
[36] Mei F, Chen D-R. Investigation of compound jet electrospray: particle encapsulation. Phys Fluids 2007;19:103303.
[37] Lee Y-H, Bai M-Y, Chen D-R. Multidrug encapsulation by coaxial tri-capillary electrospray. Colloids Surf B Biointerfaces 2011;82:104–10.
[38] Chen X, Jia L, Yin X, Cheng J, Lu J. Spraying modes in coaxial jet electrospray with outer driving liquid. Phys Fluids 2005;17:032101.
[39] Lee Y-H, Mei F, Bai M-Y, Zhao S, Chen D-R. Release profile characteristics of biodegradable-polymer-coated drug particles fabricated by dual-capillary electrospray. J Control Release 2010;145:58–65.
[40] Park J-H, Braun PV. Coaxial electrospinning of self-healing coatings. Adv Mater 2010;22:496–9.
[41] Loscertales IG, Barrero A, Guerrero I, Cortijo R, Marquez M, Gañán-Calvo AM. Micro/Nano encapsulation via electrified coaxial liquid jets. Science 2002;295:1695–8.
[42] Greiner A, Wendorff JH. Electrospinning: a fascinating method for the preparation of ultrathin fibers. Angew Chem Int Ed 2007;46:5670–703.
[43] Zhang L, Huang J, Si T, Xu RX. Coaxial electrospray of microparticles and nanoparticles for biomedical applications. Expert Rev Med Devices 2012;9:595–612.
[44] Zou W, Yu H, Zhou P, Liu L. Tip-assisted electrohydrodynamic jet printing for high-resolution microdroplet deposition. Mater Des 2019;166:107609.
[45] Yao Z-C, Wang J-C, Ahmad Z, Li J-S, Chang M-W. Fabrication of patterned three-dimensional micron scaled core-sheath architectures for drug patches. Mater Sci Eng C 2019;97:776–83.
[46] Yao Z-C, Wang J-C, Wang J-C, Ahmad Z, Li J-S, Chang M-W. A novel approach for tailored medicines: direct writing of Janus fibers. J Drug Deliv Sci Technol 2019;50:372–9.
[47] Wang B, Chen X, Ahmad Z, Huang J, Chang M-W. Engineering on-demand magnetic core–Shell composite wound dressing matrices via electrohydrodynamic micro-scale printing. Adv Eng Mater 2019;21. 1900699.
[48] Zhu L-F, Chen X, Ahmad Z, Peng Y, Chang M-W. A core–shell multi-drug platform to improve gastrointestinal tract microbial health using 3D printing. Biofabrication 2020;12:025026.